DOI: 10.1002/ange.200502336

Molecularly Assembled Nanostructures of a Redox-Active Organogelator**

Tomoyuki Akutagawa, Keiko Kakiuchi, Tatsuo Hasegawa, Sin-ichiro Noro, Takayoshi Nakamura,* Hiroyuki Hasegawa, Sinro Mashiko, and Jan Becher*

Amphiphilic molecules in solution can form a variety of molecularly assembled structures, composed, for example, of gels, micelles, vesicles, tubes, or lamellas, in a variety of dimensions, shapes, and sizes.[1–3] Several types of low-molecular-weight molecules can form organogels that generate macroscopic phase-separated molecularly assembled structures in organic solvents.[4–7] Each molecule is assembled through specific intermolecular interactions and becomes part of a fibrous structure, which is entangled to form a three-dimensional (3D) pore structure.[4–7] In general, the most important type of intermolecular interaction in an organogel is hydrogen bonding. Therefore, the molecular structure of organogelators has been limited to about 30 kinds of molecules, such as fatty acids and their monovalent salts, steroids, anthryls, amino acids, and organometallic derivatives having hydrogen-bonding sites, such as hydroxy, carboxylic, amino, and carbonyl groups.[4–7] With the exception of 2,3-bis-*n*-decyloxyanthracene,[8] organogelators have been designed

[*] Prof. T. Akutagawa, Prof. T. Hasegawa, Dr. S.-i. Noro, Prof. T. Nakamura
Research Institute for Electronic Science
Hokkaido University
Sapporo 060-0812 (Japan)
Fax: (+81) 11-706-4972
E-mail: takuta@imd.es.hokudai.ac.jp
tnaka@imd.es.hokudai.ac.jp

Prof. T. Akutagawa, K. Kakiuchi, Prof. T. Hasegawa, Dr. S.-i. Noro, Prof. T. Nakamura
Graduate Schools of Environmental and Earth Science
Hokkaido University
Sapporo 060-0810 (Japan)

Prof. T. Akutagawa, Prof. T. Nakamura
CREST, Japan Science and Technology Agency (JST)
Kawaguchi 332-0012 (Japan)

Dr. H. Hasegawa, Dr. S. Mashiko
Kansai Advanced Research Center
Communication Research Laboratory
Incorporated Administrative Agency
Kobe 651-2492 (Japan)

Prof. J. Becher
University of Southern Denmark
Campusvej 55, 5230, Odense M (Denmark)

[**] This work was partly supported by a Grant-in-Aid for Science Research from the Ministry of Education, Culture, Sports, Science, and Technology of Japan.

Supporting information for this article is available on the WWW under http://www.angewandte.org or from the author.

on the basis of their ability to participate in hydrogen-bonding interactions.

Organogelators have a tendency to form fibrous structures, which can be used to construct electrically active low-dimensional nanostructures even though most organogelators do not possess an electrically active π-electron system.[4–7] Electrically and optically active molecules, such as phthalocyanine, porphyrin, and thiophene, have been used to construct organogels through hydrogen-bonding interactions.[6,9–11] Sulfur-containing π-electron systems are useful building blocks for constructing highly electrically conducting molecularly assembled structures. For example, a variety of molecular metals and superconductors have been developed by incorporating the radical ions of tetrathiafulvalene (TTF) derivatives.[12] Organogelators incorporating S-containing π-electron systems have been reported, namely amphiphilic thiophene and TTF derivatives with hydrogen-bonding sites, which exhibit a capacity to gelate despite the absence of π–π interactions. To the best of our knowledge, the electronic properties of these organogelators have not yet been characterized. New organogelators with S-containing π-electron systems capable of self-assembling into fibrous structures through strong intermolecular S–S and π–π interactions have the potential to form electron-conducting pathways through the formation of a π-band structure. Thus, the π-stacking interaction is intrinsically a prerequisite for the formation of electrically active organogels.

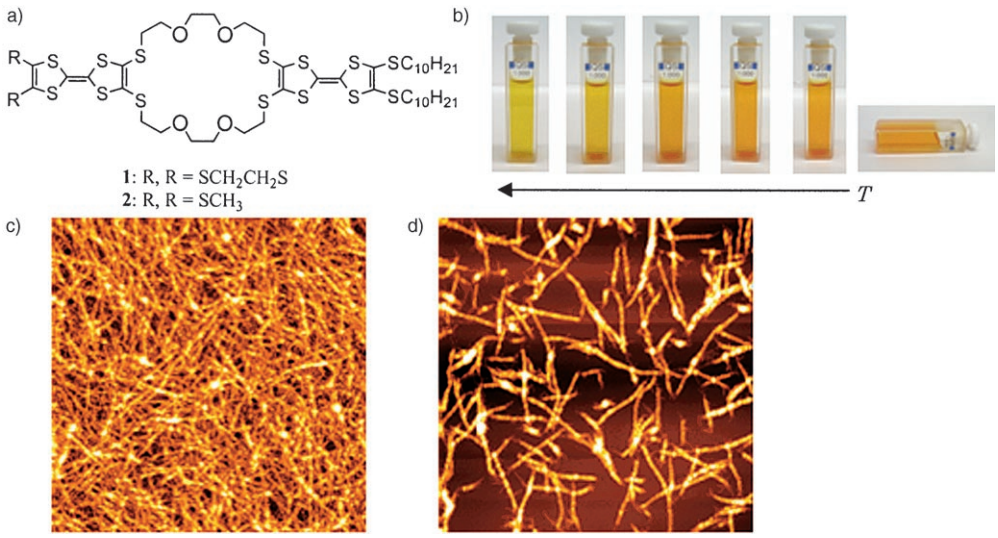

Figure 1. a) Molecular structure of amphiphilic bis-TTF annulated macrocyclic derivatives. b) Temperature-dependent organogelation of **1**. A 1 mM solution of **1** in $CHCl_3/CH_3CN$ (6/4) at 333 K was slowly cooled to 298 K. Organogelation was accompanied by a color change from yellow ($T = 333$ K) to orange ($T = 298$ K). c) Surface structure of the cast film of dried organogels on mica. d) Surface structure of a spin-coated film of dried organogels on mica. The rotational speed of the spinner was fixed at 4000 rpm. AFM images were recorded in a $10 \times 10\ \mu m^2$ scanning area.

We have constructed nanowires based on charge-transfer (CT) complexes of amphiphilic bis(tetrathiafulvalene) (bis-TTF) annulated macrocycles by molecular assembly as examples of electrically conducting nanostructures.[13,14] Formation of molecularly assembled nanowires with a typical dimension of $2.5 \times 50 \times \approx 1000\ nm^3$ has been achieved with a charge-transfer complex of a methylthio-substituted bis-TTF annulated macrocycle derivative.[2] Herein, we report a new amphiphilic bis-TTF annulated macrocycle derivative **1**, which can form redox-active organogels as well as electrically active nanostructures, such as nanowires and size-controllable nanodots (Figure 1a).

Molecule **1** was synthesized to increase the magnitude of the intermolecular interactions: a terminal ethylenedithio group ($-SCH_2CH_2S-$) effectively enhances the intermolecular interactions through lateral S–S contacts in the molecularly assembled structures compared to those in **2**, which contains methylthio groups ($-SCH_3$).[13, 14] Molecule **1** was soluble in CH_2Cl_2, $CHCl_3$, toluene, 1,2-dichloroethane, but less-soluble in CH_3CN, acetone, CH_3OH, C_2H_5OH, and *n*-hexane. Slow cooling of a solution of **1** (1 mM) in $CHCl_3/CH_3CN$ (6/4) from 333 K resulted in the generation of organogels at 293 K (Figure 1b). The yellow solution of **1** changed to an orange organogel upon cooling. The formation of organogels depended on the volume fraction of CH_3CN in the $CHCl_3/CH_3CN$ mixed solvent system. No organogels formed at room temperature at volume fractions of CH_3CN less than 40%. Other mixed-solvent systems such as $CHCl_3/CH_3OH$ (4/6), C_6H_6/CH_3CN (4/6), and $ClCH_2CH_2Cl/CH_3CN$ (4/6) also yielded organogels. However, the mixed-solvent systems of $CHCl_3/CH_3COCH_3$, $CHCl_3/C_2H_5OH$, and $CHCl_3/C_2H_5CN$ prevented formation of organogels.

Multiple hydrogen-bonding sites are the functional units that lead to one-dimensional fibrous structures in most organogelators. Although **1** possesses no hydrogen-bonding sites, the strong intermolecular π–π interactions enabled formation of an organogel. Organogelation of **1** results from replacing the terminal functional group by the ethylenedithio group since the bis(methylthio)-substituted bis-TTF annulated macrocycle **2** is incapable of forming organogels. It is known that a terminal ethylenedithio group sufficiently increases the dimensionality of intermolecular interactions through lateral interatomic S–S contacts along the peripheral direction in the π stacks.[12] Together with the π–π interaction, these intermolecular S–S interactions provide a two-dimensional electronic structure for a stable metallic and superconducting state in certain ion-radical salts of bis(ethylenedithio)-TTF.[12] Intermolecular S–S contacts of the terminal ethylenedithio group in **1** play an important role in increasing the intermolecular interaction to form fibrous structures in the organogel. The intermolecular interactions between

electrically active TTF units, which lead to a π-band structure in the solid state, are important for obtaining electrically conducting nanoscale materials.

Figure 1c,d shows organogel structures fabricated as a dried gel by cast and spin-coating techniques (1 mM $CHCl_3$/CH_3CN (6/4)), respectively, on mica. In the case of the cast film, the fibers were entangled to form a 3D structure. The film surface morphology was characteristic of an organogel:[16] introduction of organic solvents into the 3D pore yielded an organogel. By contrast, isolated fibrous structures were observed in the case of the spin-coated film. The average width and height of the fibers were 50 and 8 nm, respectively, as revealed by AFM measurements.

The fibrous shape of the organogels is conducive to constructing novel low-dimensional nanostructures. We employed the Langmuir–Blodgett (LB) technique to obtain nanostructures from organogelator **1**. Transfer of the film from the Langmuir layer on an aqueous 0.01M KCl subphase onto mica resulted in the formation of fibrous structures with an average dimension of $7 \times 70 \times$ ca. 10000 nm^3. A 2.2-nm-thick two-dimensional monolayer underlays the fibers and covers 90% of the surface area (Figure 2a). The fibers were distributed randomly on the monolayer. Although a uniform Langmuir layer was observed in the film transferred from pure water, no fiberlike domains were formed, thus suggesting that the addition of ions into the subphase contributed to the formation of the fibrous structures of donor **1** in the LB film. The addition of electrolytes, such as NaCl, NaBr, and KCl, to water decreases the surface tension of amphiphilic molecules at the air–water interface[15] as a result of the stronger adsorption of the molecules on the electrolyte-containing interface than on pure water. The decrease in the surface tension of donor **1** on the 0.01M KCl aqueous subphase accelerates the formation of micellelike molecularly assembled structures.

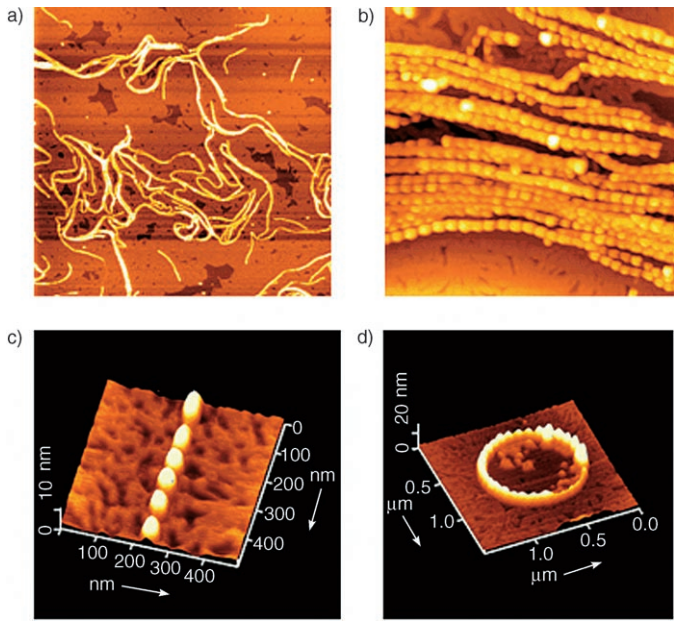

Figure 2. Surface structure of Langmuir–Blodgett films of **1** on mica. The films were fabricated by using a standard Langmuir trough at 291 K with a subphase containing 0.01 M KCl. The spreading solvent was a 0.5 mM solution of **1** in $CHCl_3$/CH_3CN (6/4) and the barrier speed was 50 $mm^2 min^{-1}$. Films were deposited by the vertical-dipping method at a constant surface pressure of 5 $mN m^{-1}$. a, b) The AFM images were recorded over an area of 10×10 and 2×2 μm^2. c, d) Expanded AFM images of a nanodot array. The nanodot-array structure has a connection of six nanodots (500×500 nm^2 image) and nanodot-ring structure is composed of about 40 nanodots (1.5×1.5 μm^2).

Each fiber was composed of a one-dimensional nanodot array (Figure 2b). The average diameter and height of the nanodots were 70 and 7 nm, respectively. The nanodots in the films often formed a regular array and ring structures (Figure 2c,d). The diameter of a nanodot ring consisting of about 40 nanodots was roughly 500 nm. The circumference of the nanodot ring (ca. 3 μm) was almost consistent with the sum of the average diameter of 40 nanodots (40×70 nm^2).

Although **1** forms nanofibers of nanodot arrays, these nanostructures are not expected to have a high electrical conductivity because of the closed-shell electronic structure. Molecule **1** shows a two-step redox behavior, with the first and second oxidation potentials at $E^1_{1/2} = 0.60$ and $E^2_{1/2} = 0.94$ V in CH_2Cl_2 (versus the saturated calomel electrode (SCE)), respectively, each of which corresponds to a two-electron ($2e^-$) oxidation reaction. The high electron-donating capacity of **1** enabled us to apply chemical oxidation by dissolving two equivalents of iodine (I_2) in a 0.5 mM solution of **1** in $CHCl_3$/CH_3CN (8/2).

The obtained CT complex of donor **1** with an open-shell electronic structure was subjected to spin coating using a drop (ca. 1 μL) of a 0.5 mM solution of **1**/$(I_2)_2$ in $CHCl_3$/CH_3CN on freshly cleaved mica. The rotational speed of the spinner was varied between 500 and 6000 rpm. Isolated nanodots were observed in spin-coated films (Figure 3a–d). No organogel was formed in the case of the 0.5 mM solution of **1**/$(I_2)_2$, thus indicating that the ability of **1** to form a fibrous structure was poor in the oxidized state. The diameter and height of the nanodots clearly depended on the rotational speed of the spinner (Figure 3e), with the nanodot diameter decreasing with increasing rotational speed. For example, the average diameter and height of the nanodots at a rotational speed of 6000 rpm were 200 and 20 nm, respectively, while those at 500 rpm were 800 and 400 nm, respectively. The diameters of the nanodots increased exponentially as the rotational speed decreases. The diameters of the nanodots can be varied from 200 to 1000 nm by adjusting the rotational speed of the spinner between 6000 and 500 rpm. The size of the nanodots can also be controlled by changing the experimental conditions, for example, the concentration of the CT complex and wetting angle of the substrate. Much smaller nanodots with a diameter of approximately 150 nm and a height of 13 nm were obtained in a diluted solution of the CT complex (0.1 mM) at a rotational speed of 4000 rpm. Small nanodots with a typical diameter of 20 nm and a height of 1.2 nm were often observed on the same spin-coated film.

The conductance of single nanodots fabricated on highly ordered pyrolytic graphite (HOPG) substrates was measured by conducting AFM (C-AFM).[16] The Pt-coated AFM tip directly contacted a single nanodot, thus forming an HOPG/nanodot/Pt sandwich. The red circles in Figure 4a at points I

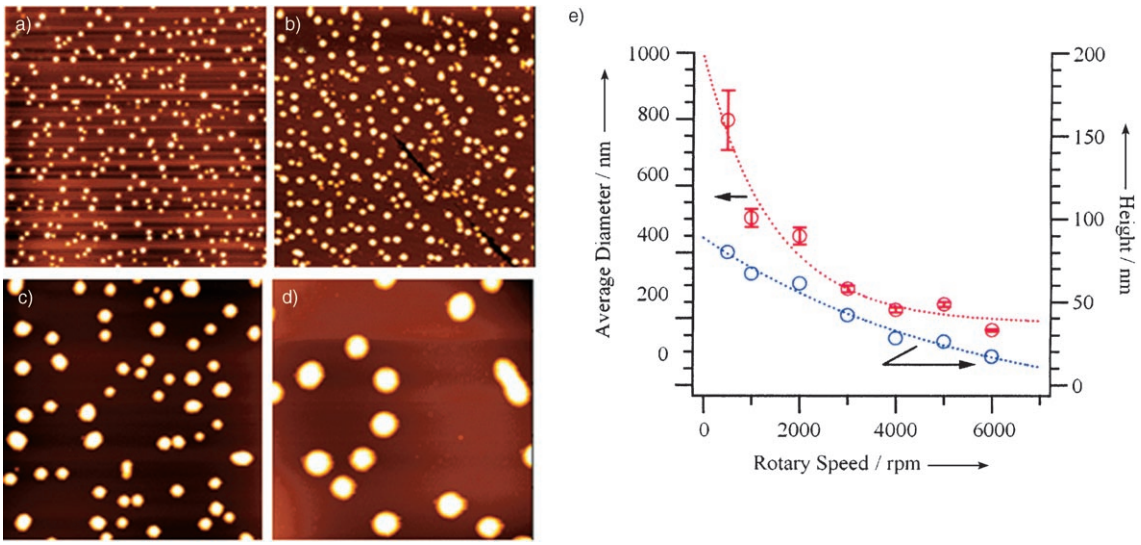

Figure 3. a–d) AFM images of size-controllable nanodots of the $\mathbf{1}/(I_2)_2$ complex with an open-shell electronic structure on mica. The rotation speed of the substrate on the spinner was 6000, 4000, 2000, and 500 rpm for (a)–(d), respectively. The scale of all AFM images is $10\times10\ \mu m^2$. e) Rotational-speed dependence of the average diameter and height of the nanodots on mica. The average diameter and height of the nanodots were obtained by statistical analysis of the AFM images ($10\times10\ \mu m^2$).

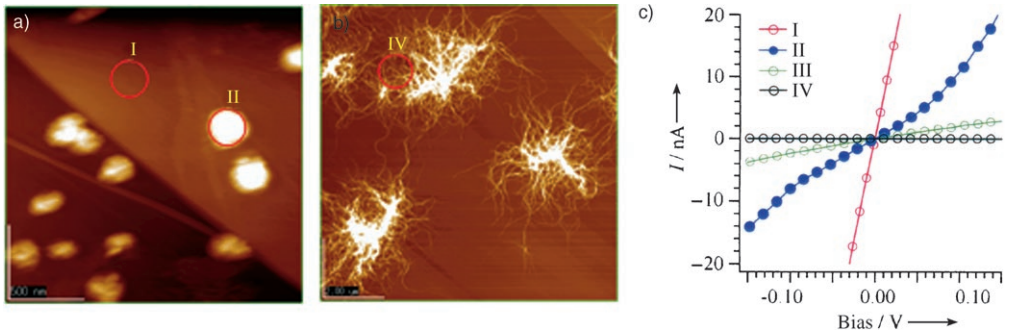

Figure 4. a) AFM image of nanodots of $\mathbf{1}/(I_2)_2$ on HOPG for conducting-AFM (C-AFM) measurements ($2\times2\ \mu m^2$). After measurement of the topological image, the Pt-coated AFM tip contacted the bare HOPG surface (point I) and a single nanodot (point II) to measure their *I–V* characteristics. The nanodot structures were retained after the conductivity measurement, as confirmed by AFM measurement. b) AFM image of fibrous structures of **1** on HOPG ($10\times10\ \mu m^2$) prepared by spin casting of a 1 mM solution ($CHCl_3/CH_3CN$ 6:4). A Pt-coated AFM tip contacted a bundle of fibers with a height of about 2 nm (point IV). c) *I–V* characteristics at points I (HOPG), II (single nanodot in air), III (single nanodot in vacuum at 5×10^{-3} Pa), and IV (bundle of fibers). DC bias was applied from −0.2 to 0.2 V.

(bare HOPG) and II (single nanodot with a diameter of 200 nm and a height of 23 nm) correspond to the contact area of the C-AFM tip during *I–V* measurements. The conductance of bare HOPG and a single nanodot were obtained from the slope of the *I–V* curve to be 730 and 20 nS, respectively, at 5×10^{-3} Pa. The conductance of the nanodot increased to 86 nS under ambient conditions because of the effects of oxygen and/or water. The fibrous structure of **1** was formed on HOPG by spin coating using a 1 mM solution of **1** in $CHCl_3/CH_3CN$ (6/4). The surface morphology shows a neuronlike network structure (Figure 4b), with the bundles of fibers randomly distributed on the HOPG. The conductance of a fiber bundle with a height of about 2 nm (point IV in Figure 4b) was about 0.03 nS, which is four to five orders of magnitude smaller than that of a single nanodot with an open-shell electronic structure. The high conductance of single nanodots of the CT complex reflect the high concentration of the conduction carriers.

In conclusion, a new organogelator consisting of an amphiphilic bis-TTF annulated macrocyclic derivative was synthesized. The terminal ethylenedithio group increased the intermolecular interactions through lateral S–S contacts, in addition to the π–π interaction, which was responsible for organogelation. A three-dimensional entangled structure of fibers was confirmed in the dried organogel. The organogelator produced nanodot-array structures in Langmuir–Blodgett films. The chemically oxidized organogelator formed size-controllable isolated nanodot structures, which were simply fabricated by the spin-coating technique. The size of the nanodots depended on the rotational speed of the substrate, and was thus controllable. The conductance of a single nanodot with an open-shell electronic structure was four to five orders of magnitude higher than that of fibers of **1** with a closed-shell electronic structure. Nanostructures of molecular conductors can potentially be used in molecular electronic devices as electrically active units.

Experimental Section

1: Donor **1** was synthesized by a stepwise protection/deprotection protocol of the cyanoethylene groups. 2-Iodoethoxyethane was introduced into ethylenedithiolo-bis(2-cyanoethylthio)TTF by deprotection of a cyanoethylene group, then treated under high-dilution conditions in DMF. The [24]crown-8 macrocycle was formed by addition of two equivalents of CsOH to the bis(TTF) compound, which yielded the amphiphilic bis(TTF) annulated macrocycle **1**. The **1**/$(I_2)_2$ complex was prepared in situ by mixing donor **1** and two equivalents of I_2 in $CHCl_3/CH_3CN$ (8/2, v/v). The concentration of the CT complex solution was fixed at 0.5 mM with respect to **1**/$(I_2)_2$.

The spin-coated films were produced on a mica surface ($10 \times 10\ mm^2$) by adjusting the rotational speed from 500 to 6000 rpm. About 1 μL of the CT complex solution was dropped onto the rotating mica surface, which was rotated for a further 60 s. The floating monolayers were left for 30 min after spreading of the CT complex (NIMA633 D2/D1). The LB monolayers were transferred onto freshly cleaved mica surfaces at a fixed surface pressure of $10\ mN\,m^{-1}$ by a single up-stroke.

Dynamic mode AFM images were recorded on a Seiko SPA 400 with an SPI 3800 probe station and JEOL JSPM-5200. Commercially available Si cantilevers with a force constant of $13\ N\,m^{-1}$ were used. *I–V* characteristics of the nanodots were measured by direct contact of the Pt-coated AFM tip with single nanodots on the HOPG surface.

Received: July 5, 2005
Published online: October 17, 2005

Keywords: conducting materials · gels · molecular electronics · nanostructures · thin films

[1] J. N. Israelachvili, *Intermolecular and Surface Forces*, Academic Press, London, **1992**.
[2] G. William, O. Leonard, J. Barbour, J. L. Atwood, *Science* **1999**, *285*, 1049 – 1052.
[3] S. I. Stupp, V. LeBonheur, K. Walker, L. S. Li, K. E. Huggins, M. Keser, A. Amstutz, *Science* **1997**, *276*, 384 – 389.
[4] P. Terech, R. G. Weiss, *Chem. Rev.* **1997**, *97*, 3133 – 3159.
[5] L. A. Estroff, A. D. Hamilton, *Chem. Rev.* **2004**, *104*, 1201 – 1218.
[6] D. J. Abdallah, R. G. Weiss, *Adv. Mater.* **2000**, *12*, 1237 – 1247.
[7] O. Gronwald, E. Snip, S. Shinkai, *Curr. Opin. Colloid Interface Sci.* **2002**, *7*, 148 – 156.
[8] F. Placin, M. Colomès, J.-P. Desvergne, *Tetrhadron Lett.* **1997**, *38*, 2665 – 2668.
[9] a) M. Jörgensen, K. Bechgaard, T. Björnholm, P. Sommer-Larsen, L. G. Hansen, K. Schaumburg, *J. Org. Chem.* **1994**, *59*, 5877 – 5882; b) T. L. Gall, C. Pearson, M. R. Bryce, M. C. Petty, H. Dahlgaard, J. Becher, *Eur. J. Org. Chem.* **2003**, 3562 – 3568.
[10] C. F. van Nostrum, S. J. Picken, A.-J. Schouten, R. J. M. Nolte, *J. Am. Chem. Soc.* **1995**, *117*, 9957 – 9965.
[11] F. S. Schoonbeek, J. H. van Esch, B. Wegewijs, D. B. A. Rep, M. P. de Haas, T. M. Klapwijk, R. M. Kellogg, B. L. Feringa, *Angew. Chem.* **1999**, *111*, 1486 – 1490; *Angew. Chem. Int. Ed.* **1999**, *38*, 1393 – 1397.
[12] T. Ishiguro, K. Yamaji, G. Saito, *Organic Superconductors*, Springer, New York, **1998**.
[13] T. Akutagawa, T. Ohta, T. Hasegawa, T. Nakamura, C. A. Christensen, J. Becher, *Proc. Natl. Acad. Sci. USA* **2002**, *99*, 5028 – 5033.
[14] T. Akutagawa, K. Kakiuchi, T. Hasegawa, T. Nakamura, C. A. Christensen, J. Becher, *Langmuir* **2004**, *20*, 4187 – 4195.
[15] P. Mukerjee, *J. Phys. Chem.* **1965**, *69*, 4038 – 4040.
[16] T. W. Kelley, E. L. Granstrom, C. D. Frisbie, *Adv. Mater.* **1999**, *11*, 261 – 264.

